

A unified large/small-scale dynamo in helical turbulence

Pallavi Bhat^{1,2*}, Kandaswamy Subramanian^{1†}, and Axel Brandenburg^{3,4,5,6‡}

¹*Inter University Centre for Astronomy and Astrophysics, Post Bag 4, Pune University Campus, Ganeshkhind, Pune 411 007, India*

²*Department of Astrophysical Sciences and Princeton Plasma Physics Laboratory, Princeton University, Princeton, NJ 08540, USA*

³*Nordita, KTH Royal Institute of Technology and Stockholm University, Roslagstullsbacken 23, SE-10691 Stockholm, Sweden*

⁴*Department of Astronomy, AlbaNova University Center, Stockholm University, SE-10691 Stockholm, Sweden*

⁵*JILA and Department of Astrophysical and Planetary Sciences, University of Colorado, Boulder, CO 80303, USA*

⁶*Laboratory for Atmospheric and Space Physics, University of Colorado, Boulder, CO 80303, USA*

5 August 2021

ABSTRACT

We use high resolution direct numerical simulations (DNS) to show that helical turbulence can generate significant large-scale fields even in the presence of strong small-scale dynamo action. During the kinematic stage, the unified large/small-scale dynamo grows fields with a shape-invariant eigenfunction, with most power peaked at small scales or large k , as in Subramanian & Brandenburg (2014). Nevertheless, the large-scale field can be clearly detected as an excess power at small k in the negatively polarized component of the energy spectrum for a forcing with positively polarized waves. Its strength \overline{B} , relative to the total rms field B_{rms} , decreases with increasing magnetic Reynolds number, Re_M . However, as the Lorentz force becomes important, the field generated by the unified dynamo orders itself by saturating on successively larger scales. The magnetic integral scale for the positively polarized waves, characterizing the small-scale field, increases significantly from the kinematic stage to saturation. This implies that the small-scale field becomes as coherent as possible for a given forcing scale, which averts the Re_M -dependent quenching of $\overline{B}/B_{\text{rms}}$. These results are obtained for 1024^3 DNS with magnetic Prandtl numbers of $\text{Pr}_M = 0.1$ and 10 . For $\text{Pr}_M = 0.1$, $\overline{B}/B_{\text{rms}}$ grows from about 0.04 to about 0.4 at saturation, aided in the final stages by helicity dissipation. For $\text{Pr}_M = 10$, $\overline{B}/B_{\text{rms}}$ grows from much less than 0.01 to values of the order the 0.2 . Our results confirm that there is a unified large/small-scale dynamo in helical turbulence.

Key words: MHD–dynamo–turbulence–galaxies:magnetic fields–Sun:dynamo–magnetic fields

1 INTRODUCTION

Astrophysical systems like stars and galaxies host magnetic fields that are coherent on the scale of the system itself. These fields are thought to arise due to the action of a turbulent dynamo, whereby helical turbulence combined with shear amplifies and maintains fields coherent on scales larger than the scales of random stirring. Indeed, the scales of the stirring like convective scale in the Sun or the supernova-induced turbulent scales in galaxies, are much smaller than the coherence scale of the large-scale field. A dynamo which amplifies fields on scales larger than that of the stirring is referred to as a large-scale or mean-field dynamo.

There are two major potential difficulties associated

with mean-field dynamos. One is that small-scale helical fields which are produced during mean-field dynamo action, due to magnetic helicity conservation, go to quench the dynamo. Thus, they have to be eliminated from the dynamo active region by some form of magnetic helicity flux, to avoid such quenching (Brandenburg & Subramanian 2005; Brandenburg et al. 2012; Blackman 2015). Equally important is the fact that, while mean-fields are being generated, the same turbulence, for a large enough magnetic Reynolds number, Re_M , also generically lead to the small-scale or fluctuation dynamo. The fluctuation dynamo rapidly generates magnetic fields coherent on scales of the order of or smaller than the outer scales of the turbulence, and in principle, at a rate faster than the mean fields (Kazantsev 1968; Kulsrud & Anderson 1992; Subramanian 1999; Haugen et al. 2004; Schekochihin et al. 2004; Brandenburg & Subramanian 2005; Tobias et al. 2011; Brandenburg et al. 2012). The question then arises as

* E-mail: palvi@iucaa.ernet.in

† kandu@iucaa.in

‡ E-mail: brandenb@nordita.org

to whether and how the mean-field dynamo operates in the presence of such rapidly growing magnetic fluctuations.

This issue was partially addressed by Subramanian & Brandenburg (2014) (hereafter SB14), through direct numerical simulations (DNS) and by analyzing the Kazantsev (1968) model, focusing on the kinematic regime. They showed that in this regime, the magnetic energy spectrum grows as an eigenfunction, i.e. at each wavenumber k the spectrum grows with the same growth rate. Nevertheless, there is indeed evidence for this large-scale field generation in the horizontally averaged large-scale field, which can also be seen as excess power at small k in one of the oppositely helically polarized components. However, they also found that the relative strength of the large-scale or mean-field component compared to the rms field, in the kinematic stage, decreases with increasing Re_M like $\text{Re}_M^{-3/4}$ for larger values of Re_M . From both an analysis of the Kazantsev model including helicity (Kazantsev 1968; Vainshtein & Kichatinov 1986; Subramanian 1999; Boldyrev et al. 2005) and the DNS, SB14 showed that this is a result of the magnetic energy spectrum peaking on small resistive scales even in the presence of helicity. If such a feature persisted on saturation, it would be difficult to explain the prevalence of large-scale fields. Of course, as the dynamo-generated field grows, the Lorentz force will become important, first at small scales, and saturate the growth of small-scale fields. It is then important to determine whether the mean-field dynamo can continue to grow large-scale fields as the fluctuation dynamo saturates. And can this large-scale field become more dominant at saturation, independent of Re_M ? Our aim in this paper is to answer these questions.

For this purpose we have run DNS of magnetic field growth in helically driven turbulence in a periodic domain, with resolutions up to 1024^3 mesh points. These simulations are designed to adequately capture the dynamics of scales both smaller and larger than the forcing scale, and run from the kinematic regime to nonlinear saturation. The next section presents the simulations that we have carried out to use for our analysis. Section 3 sets out the results of our analysis to determine the evolution of both the large- and small-scale fields generated by helical turbulence. Section 4 presents a discussion of these results and the last section, our conclusions.

2 SIMULATING LARGE-SCALE DYNAMOS

To study the growth of the large-scale or mean-field dynamo in the presence of a small-scale or fluctuation dynamo, we have run a suite of simulations of helically driven turbulence using the PENCIL CODE¹ (Brandenburg & Dobler 2002; Brandenburg 2003). The continuity, Navier-Stokes and induction equations are solved in a Cartesian domain of a size $(2\pi)^3$ on a cubic grid with N^3 mesh points, adopting triply periodic boundary conditions. The fluid is assumed to be isothermal, viscous, electrically conducting and mildly

Table 1. Summary of runs discussed in this paper. Here the values of u_{rms} are from kinematic phase, whereas B_{rms} and \overline{B} refer to values from the saturation phase after ~ 624 eddy turnover times for Runs A, B, and C and after ~ 463 eddy turnover times for Runs D, E, and F; the eddy turn over time is given by $1/(u_{\text{rms}}k_f)$.

Run	Pr_M	Re_M	u_{rms}	B_{rms}	\overline{B}	$\overline{B}/B_{\text{rms}}$	N^3
A	0.1	330	0.135	0.085	0.033	0.38	1024^3
B	0.1	160	0.130	0.092	0.046	0.49	256^3
C	0.1	65	0.130	0.092	0.055	0.59	256^3
D	10	3375	0.135	0.078	0.017	0.22	1024^3
E	10	1575	0.126	0.072	0.019	0.27	256^3
F	10	665	0.133	0.082	0.026	0.32	256^3

compressible. The governing equations are given by,

$$\frac{D}{Dt} \ln \rho = -\nabla \cdot \mathbf{u}, \quad (1)$$

$$\frac{D}{Dt} \mathbf{u} = -c_s^2 \nabla \ln \rho + \frac{1}{\rho} \mathbf{J} \times \mathbf{B} + \mathbf{F}_{\text{visc}} + \mathbf{f}, \quad (2)$$

$$\frac{\partial}{\partial t} \mathbf{A} = \mathbf{u} \times \mathbf{B} - \eta \mu_0 \mathbf{J}. \quad (3)$$

Here ρ is the density related to the pressure by $P = \rho c_s^2$, where c_s is speed of sound. The operator $D/Dt = \partial/\partial t + \mathbf{u} \cdot \nabla$ is the Lagrangian derivative, where \mathbf{u} is fluid velocity field. The induction equation is being expressed in terms of the vector potential \mathbf{A} , so that $\mathbf{B} = \nabla \times \mathbf{A}$ is the magnetic field, $\mathbf{J} = \nabla \times \mathbf{B}/\mu_0$ is the current density and μ_0 is the vacuum permeability ($\mu_0 = 1$ in the DNS). The viscous force is given as $\mathbf{F}_{\text{visc}} = \rho^{-1} \nabla \cdot 2\nu \rho \mathbf{S}$, where ν is the kinematic viscosity, and \mathbf{S} is the traceless rate of strain tensor with components $S_{ij} = \frac{1}{2}(u_{i,j} + u_{j,i}) - \frac{1}{3}\delta_{ij} \nabla \cdot \mathbf{u}$. Here commas denote partial derivatives. The forcing term $f = f(\mathbf{x}, t)$ is responsible for generating turbulent helical flow. The forcing is maximally helical as described in SB14. In Fourier space, this driving force is transverse to the wavevector \mathbf{k} and localized in wavenumber space about a wavenumber k_f . It drives vortical motions in a wavelength range around $2\pi/k_f$, which will also be the energy carrying scales of the turbulent flow. The direction of the wavevector and its phase are changed at every time step in the simulation making the force δ -correlated in time; see Brandenburg (2001); Haugen et al. (2004); Subramanian & Brandenburg (2014) for details.

For all our simulations, we choose to drive the motions at a wavenumber $k_f = 4$. This choice is motivated by the fact that we wish to resolve both the small-scale magnetic field structures in any turbulent cell and at the same time include scales larger than the flow (with $k < k_f$). The strength of the forcing is adjusted so that the rms Mach number of the turbulence, u_{rms} in the code (where velocity is measured in units of the isothermal sound speed), is typically about 0.1. This small value implies also that the motions are nearly incompressible. We define the magnetic and fluid Reynolds number respectively by $\text{Re}_M = u_{\text{rms}}/\eta k_f$ and $\text{Re} = u_{\text{rms}}/\nu k_f$, where η and ν are the resistivity and viscosity of the fluid. The magnetic Prandtl number is defined as $\text{Pr}_M = \text{Re}_M/\text{Re} = \nu/\eta$.

For the simulations reported here we take $\text{Pr}_M = 0.1$

¹ <https://github.com/pencil-code>

and $\text{Pr}_M = 10$; the former value was used in most of the DNS in SB14. This was motivated by the fact that for such small values of Pr_M , the non-helical small-scale dynamo was expected to be much harder to excite (Iskakov et al. 2007), which would then provide a better chance of seeing evidence for the large-scale field in the kinematic stage. SB14 however found an efficient small-scale dynamo even for $\text{Pr}_M = 0.1$. This is related to the fact that in SB14 the forcing wavenumber was chosen to be $k_f = 4$, while in the earlier work of Iskakov et al. (2007) it was between 1 and 2. Furthermore, the disappearance of the small-scale dynamo for $k_f = 1.5$ is related to the bump in the spectrum near the dissipation wavenumber, which is known as the ‘‘bottleneck phenomenon’’ (Falkovich 1994). In the nonlinear regime, however, this bump is suppressed by the magnetic field and therefore the strength of the small-scale dynamo is nearly independent of Pr_M (Brandenburg 2011). As we would like to compare with the kinematic results of SB14 and extend it to the nonlinear regime, we consider first the value of $\text{Pr}_M = 0.1$. For both values of Pr_M , we have studied a range of Re_M . The fiducial simulation of a helical dynamo considered in this paper has a resolution of 1024^3 mesh points and $\text{Re}_M = 330$ (hence $\text{Re} = 3300$), which we from now on refer to as Run A. The other run with a similar resolution of 1024^3 mesh points has $\text{Pr}_M = 10$ and is referred to as Run D. A summary of different runs used in this paper is given in Table 1.

A quantity that was also evaluated in the DNS of SB14 and which helps to understand how the growth rate of the fluctuation dynamo changes as compared to the mean-field dynamo is the growth rate as a function of k , $\lambda(k)$, of the magnetic energy residing in each k defined in the following manner. We first extract the evolution of magnetic energy at a given k , $M_k(t)$ from $E_M(k, t)$ and perform a running average with a suitable window, to smooth the evolution curve, $\bar{M}_k(t)$. This window is chosen such that the smoothing reduces the noise sufficiently but at the same time does not produce any new false features in the curve. Subsequently, to determine λ , we take the logarithmic derivative given by

$$\lambda = \frac{1}{M_k(t)} \frac{dM_k(t)}{dt}. \quad (4)$$

We determine the λ for each k , to obtain $\lambda(k)$.

3 RESULTS

We first consider the results from one of our higher resolution simulations of a turbulent helical dynamo with 1024^3 mesh points (fiducial Run A) from the kinematic stage up to nonlinear saturation. Most of our results have been obtained using the spectral data from the DNS.

3.1 The evolution of spectra

In Figure 1, we show the evolving kinetic and magnetic energy spectra, $E_K(k)$ and $E_M(k)$, of the helically driven dynamo, in dotted blue and solid black lines respectively. For a maximally helical velocity field, the mean-field α^2 dynamo in a periodic box, is expected to grow fields initially at a wavenumber $k = k_f/2 = 2$ (see Brandenburg et al. (2002) and SB14), which will then move to even larger scales

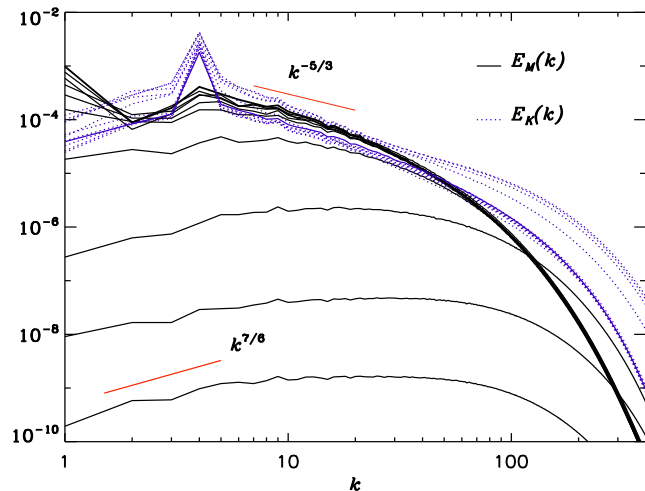


Figure 1. Evolution of $E_M(k, t)$ for Run A (solid black lines) together with $E_K(k, t)$ (dotted blue), with the final curve in solid blue. The spectra are at regular intervals of 100 code time units, starting at $t = 100$.

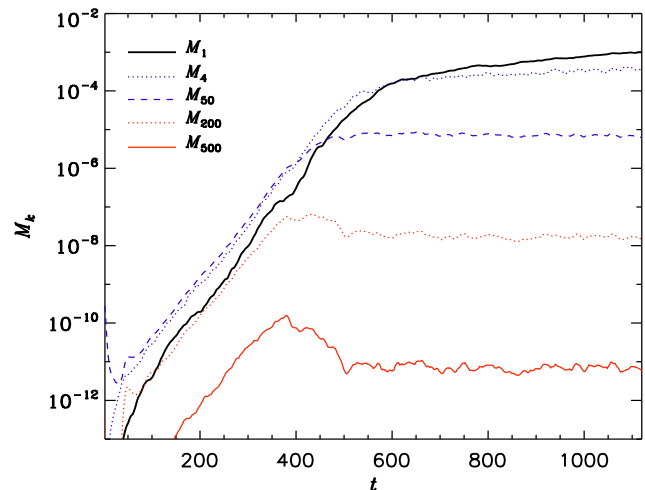


Figure 2. Evolution of $M_k(t)$ for $k = 1, 4, 50, 200,$ and 500 has been shown for Run A.

(smaller k) in the saturated state (Brandenburg 2001). On the other hand, the fluctuation dynamo is expected to be active at scales equal to and below the forcing scale (larger wavenumbers). In the early kinematic stage, a single common eigenfunction is seen growing in a self similar manner, with the magnetic energy spectrum $E_M(k, t)$ increasing towards the smaller resistive scales. This is similar to what is seen in the DNS of large-scale dynamo action by SB14, during the kinematic stage. Also the slope of $E_M(k)$ is close to $k^{7/6}$, which agrees with a result derived by SB14 using Kazantsev model including helicity.

At late times, when the dynamo saturates, the slope of $E_M(k, t)$ as a function of k flattens first, with the peak of the spectrum shifting secularly to smaller and smaller wavenumbers (larger and larger scales). The subsequent saturated spectra develop two peaks, one at the forcing scale and another at the largest scale or smallest wavenumber, $k = k_1 = 1$.

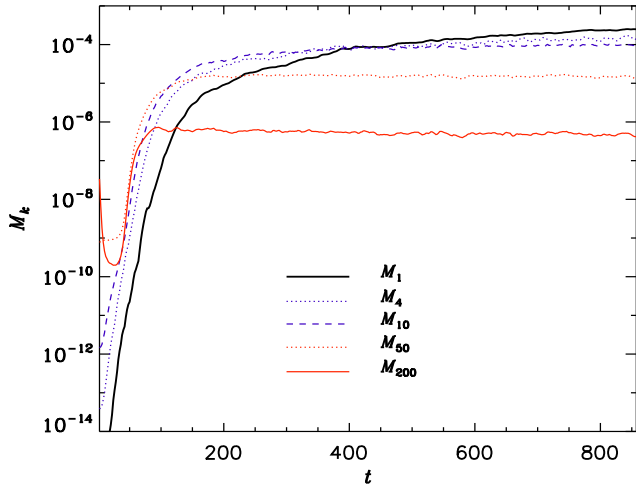


Figure 3. Evolution of $M_k(t)$ for $k = 1, 4, 10, 50,$ and 200 has been shown for Run D.

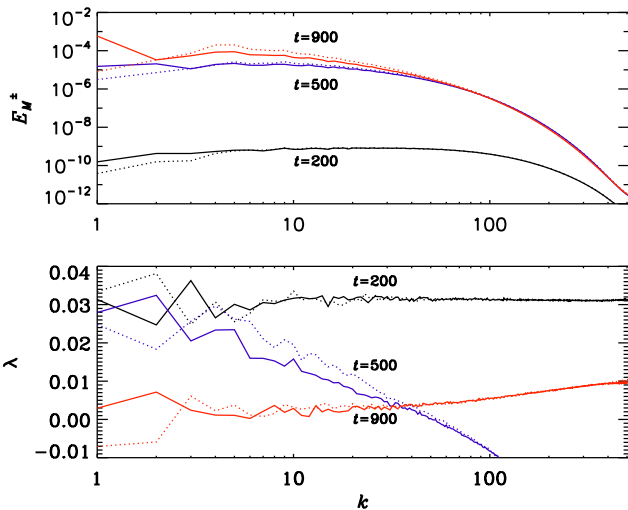


Figure 4. In the top panel, spectra of E_M^- for Run A are in solid curves and E_M^+ are in dotted curves at three times, $t = 200, 500,$ and 900 . In the bottom panel the corresponding growth rate, $\lambda(k)$ is shown.

To make this saturation behavior clearer, we show for Run A in Figure 2 the evolution of magnetic energy residing in different scales. The evolution of M_k is shown for wavenumbers $k = 1, 4, 50, 200,$ and 500 . It can be seen that M_k first grows almost exponentially with similar slopes for all k in the kinematic stage, before saturating. For higher wavenumbers, M_k stops growing and turns to saturate at lower strengths, and earlier than magnetic energy at lower wavenumbers. The M_4 and M_{50} modes (dotted blue and dashed blue lines), turn to saturate at around $t = 525$ and 450 , respectively, as compared to M_1 in solid black, which has not saturated even at late times. In fact, the M_1 mode, which reflects the operation of the large-scale dynamo, is seen to be still growing, and has a distinctive positive slope compared to the saturated flatter curves at other wavenumbers.

A similar picture is seen also for Run D ($\text{Pr}_M = 10$), as shown in Figure 3. Here, the growth rate is much larger

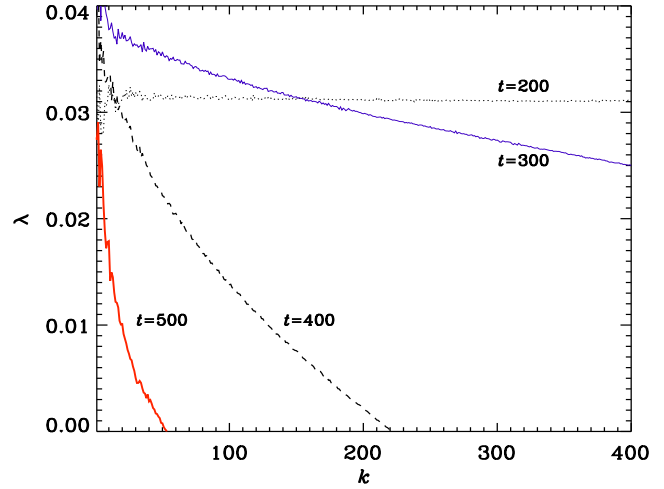


Figure 5. Growth rate $\lambda(k)$ for Run A as a function of k at times $t = 200, 300, 400,$ and 500 .

than for Run A ($\text{Pr}_M = 0.1$). This is because for $\text{Pr}_M > 1$ (and also large Re_M), firstly, the smallest eddies whose scale-dependent Re_M is greater than the critical value for small-scale dynamo action, have a shorter turnover time. Secondly, the larger value of Re_M for Run D (by an order of magnitude, compared to the $\text{Pr}_M = 0.1$ run), could make the dynamo in that run more efficient – even for a similar eddy turnover rate. Thus, the helical dynamo in Run D turns to saturate at a much earlier time compared to Run A. As is well known starting from the work of Brandenburg & Subramanian (2001) (see also Brandenburg & Subramanian (2005); Brandenburg et al. (2012); Blackman (2015) for reviews), this growth of large-scale field requires small-scale helicity to be lost from the system. In the present context of a completely homogeneous dynamo with uniform energy density of the large-scale field, such a loss is purely due to resistivity, whereas more realistically it would be aided by helicity fluxes out of the dynamo active region. Nevertheless, the magnetic field evolution reflected in Figures 1 and 2 goes to show that even after the fluctuation dynamo saturates, the mean-field dynamo continues to grow large-scale fields, provided also that small-scale magnetic helicity can be lost.

An interesting behavior to note is that the M_1 mode is growing together with all other modes at about the same rate and turns off to saturate almost along with M_4 . From this a picture emerges where there is one unified large- and small-scale dynamo in such helical turbulence (Subramanian 1999), which simply grows fields on all scales together, and saturates at successively larger and larger scales (smaller and smaller wavenumbers). We return to this idea below.

3.2 Polarization spectra and wavenumber dependent growth rate

For the large-scale dynamo action which arises in helical turbulence, the turbulent emf, in a two-scale model, is expected to generate oppositely signed small- and large-scale magnetic helicities. Thus, one way of distinguishing large- and small-scale fields would be to compute spectra from the field split into positively and negatively po-

larized components, defined as (Brandenburg et al. 2002; Brandenburg & Subramanian 2005)

$$E_M^\pm(k, t) = \frac{1}{2} \left[E_M(k, t) \pm \frac{1}{2} k H_M(k, t) \right]. \quad (5)$$

This would enable one to see a clearer signature of the large-scale field and its evolution from the kinematic stage to non-linear saturation. In the top panel of Figure 4, we show for Run A the spectrum of the two oppositely polarized field components (depending on helicity), $E_M^\pm(k, t)$, at three times, $t = 200, 500$, and 900 . The spectra of the negatively polarized field, $E_M^-(k, t)$, are shown as solid lines and those of the positively polarized field are shown as dotted lines. Also the continuous ordering of the field, and the continued growth of large-scale field even when the small-scale field saturates, can also be seen by examining the wavenumber-dependent growth rate, $\lambda(k)$. In the bottom panel of Figure 4, the growth rates $\lambda(k)$ corresponding to $E_M^\pm(k, t)$ have been plotted. The black curves in both panels are at $t = 200$, in the kinematic stage. We see that at this time $\lambda(k)$ is nearly uniform across k in both polarized components, indicating in the presence of an eigenfunction which is growing at the same rate at all scales, both large and small. (This can also be seen from Figure 5.) We see that both polarized spectra extend over all k , and in fact overlap at large k , indicating that the magnetic field has little helicity on such large k . However even at this time, there is an excess of power in the negatively polarized field at small k , indicating the presence of a large-scale field due to the mean-field dynamo, as also found in SB14.

The blue curves at $t = 500$, in the top panel, show that the negatively polarized (large-scale) field (given by the solid line) near small k is starting to rise above the rest of the spectrum. Correspondingly we see from the bottom panel that the growth rate of the negatively polarized large-scale field component (solid curve) peaks at small k , whereas that of the positively polarized field (the dotted line) peaks at around $k = 4$. Furthermore, there is a decrease in λ for the rest of the spectrum. This can also be noted from Figure 5, where the $\lambda(k)$ at $t = 500$ for large k had decreased significantly as compared to when $t = 200$ or $t = 300$. Note that the peak in $\lambda(k)$ at $k = 2$ for the negatively polarized component, is consistent with the expectation that a fully helical α^2 mean-field dynamo grows fields at $k = k_f/2$.

Therefore, at these later times, there is no longer a growing eigenfunction. Instead, the field is beginning to order itself both on large scales (due to the helical large-scale dynamo) and also now on the forcing scale (due to the small-scale dynamo modified by the Lorentz force). Finally, at $t = 900$, shown as the red curves, the energy in the large-scale fields ($E_M^-(k, t)$ given by the solid line) shows a peak at k_1 as seen in the top panel. In the bottom panel, we see that the growth rate for both polarizations are close to 0, but the negatively polarized large-scale field (solid curve) still shows a positive λ at small k . Thus, at this time the small-scale field has saturated, but the large-scale field continues to grow in the presence of a saturated small-scale dynamo (albeit due to the loss of helicity through resistivity; see below).

3.3 Evolution of the small-scale field coherence

As our work is focused on the evolution of the large-scale field in the presence of growing small-scale fields, it is also

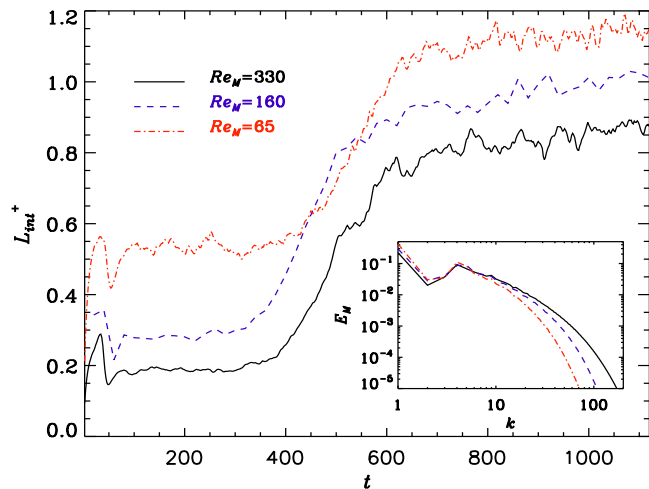


Figure 6. Evolution of the integral scale L_{int}^+ for Runs A, B, and C. In the inset, their respective normalized saturated final magnetic spectra are shown.

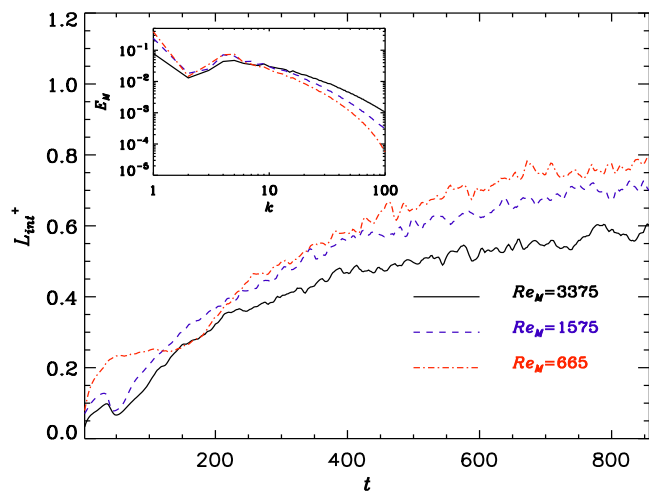


Figure 7. Evolution of the integral scale L_{int}^+ for Runs D, E, and F. In the inset, their respective normalized saturated final magnetic spectra are shown.

of interest to examine the evolution of coherence properties of the small-scale field. It is well known that the non-helically driven fluctuation dynamo generates fields whose power is concentrated on resistive scales in the kinematic stage. We have seen from our DNS (and from the work of SB14) that this continues to hold even when the turbulence is helical. In fact, in the kinematic stage, the spectrum is dominated by power which is concentrated at resistive scales due to the fluctuation dynamo. For a high- Re_M system, if such a feature persisted in saturation, the prevalence of a mean field would be questionable. Thus, it is important to investigate whether for a high- Re_M system, there is a shift of magnetic energy from resistive scales to larger scales closer to the stirring scale on saturation. To address this question, we show in Figure 6, the time evolution of the integral scale of the positively polarized spectrum (which is predominantly the small-scale field), for Run A. Similar results were obtained if we define the energy spectrum of the small-scale field to be

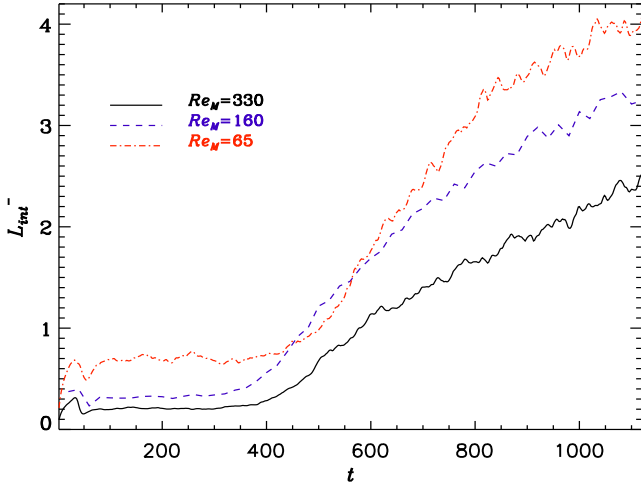


Figure 8. Evolution of the integral scale, L_{int}^- , of the negatively polarized $E_M^-(k)$ characterizing the large-scale dynamo, is shown for Runs A, B, and C, corresponding to $\text{Re}_M = 330$, 160, and 65, respectively.

$E_M(k, t)$ with $k > k_f$. This integral scale, defined here separately for positively and negatively polarized components, is given by

$$L_{\text{int}}^\pm(t) = \frac{\int (2\pi/k) E_M^\pm(k, t) dk}{\int E_M^\pm(k, t) dk}. \quad (6)$$

In the following, we are particularly interested in $L_{\text{int}}^+(t)$, which characterizes the small-scale part of the field. In Figure 6, the integral scale for the fiducial high resolution Run A is shown as a solid black line. We also show the results from two lower resolution runs, Runs B and C, with $\text{Pr}_M = 0.1$. In Figure 7, we show the results from Runs D, E, and F, all of which have $\text{Pr}_M = 10$.

For the fiducial run, we see that the integral scale is roughly constant at $L_{\text{int}}^+ \sim 0.17$ during the kinematic stage, reflecting the fact that the positively polarized field grows as an eigenfunction during this stage, with a small coherence scale. However, as the Lorentz force becomes important, $L_{\text{int}}^+(t)$ begins to increase rapidly. This process begins at $t \sim 400$, which is also the time when the large k modes ($k > 50$) stop growing (see Figures 1 and 2). This rapid increase stops at $t \sim 600$ and $L_{\text{int}}^+ \sim 0.8$, when the small-scale field modes with $k = k_f$ have largely saturated. There is then a subsequent slower rise of L_{int}^+ to ~ 0.9 , as the large-scale field starts to dominate. Thus, there is considerable increase (by more than a factor 5) in the integral scale of the small-scale field from the kinematic to the saturated state. This factor is higher than that of ~ 3 seen for fluctuation dynamo in the purely nonhelical case, albeit for $\text{Pr}_M = 1$ (Bhat & Subramanian 2013). In the case of $\text{Pr}_M = 10$, as for Run D, L_{int}^+ increases from a value of ~ 0.075 in the kinematic stage to ~ 0.6 at saturation, which is an increase by a factor of ~ 8 .

Similar evolutions are also seen at lower Re_M . However here L_{int}^+ is larger even in the kinematic state (reflecting the smaller resistive wavenumber for a lower Re_M). And L_{int}^+ also saturates at a larger value for a lower Re_M , reflecting the fact that the spectrum cuts off at smaller k for lower Re_M . This latter feature can be seen from the normalized spectra shown

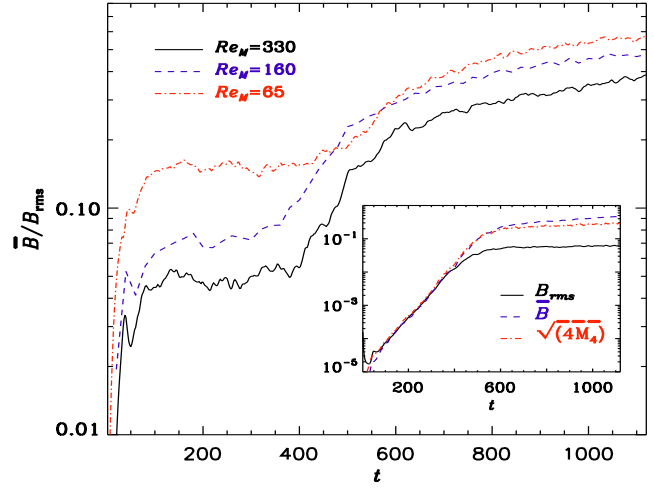


Figure 9. The ratio $\overline{B}/B_{\text{rms}}$ is evolving with time, for Runs A, B, and C. In the inset panel, for Run A, the three curves of $B_{\text{rms}}(t)$, $\overline{B}(t)$ and $\sqrt{4M_k}$ for $k = 4$ are shown separately, where the latter two curves are scaled by a constant to make all curves overlap in the kinematic stage.

in the inset of Figure 6. Also note that, even though the saturated L_{int}^+ is slightly different for Runs A, B, and C, in all three cases, the peak power for the saturated small-scale dynamo is always at the forcing scale, $k_f = 4$. In fact, one can also compare the L_{int}^+ obtained for our fiducial run with that expected for a small-scale field coherent on the scale of forcing. Suppose we modelled the spectrum of this field as $E_M^+ = M_0(k/k_f)^2$ for $k < k_f$ and $E_M^+ = M_0(k/k_f)^{-5/3}$ for $k > k_f$, then one gets $L_{\text{int}}^+ = 0.6(2\pi/k_f) = 0.94$, which compares reasonably well with that obtained in our highest resolution run. Thus, it appears that, on saturation, the small-scale field at the given forcing scale has become almost as coherent as possible. Note that, if the power in the small-scale fields were still at resistive scales, any peak in $E_M(k, t)$ at $k = 1$ would have made negligible contribution to B_{rms} . Therefore, the above result provides some assurance that, even in high Re_M systems, the large-scale field can indeed be significant and reveal itself on saturation.

In the Figure 8, we also show the evolution of L_{int}^- (for the large scale field) for the runs with $\text{Pr}_M = 0.1$. In the kinematic regime, these curves are only slightly higher in amplitude compared to the corresponding L_{int}^+ curves in Figure 6, thus indicating the slight excess in energy at large scales. Around the same time as L_{int}^+ , the L_{int}^- curves start increasing to higher values. For Run A, L_{int}^- increases from 0.17 to a value of 2.5 which is about factor of 3 larger than the final L_{int}^+ . The difference in the final values between the three curves for different Re_M is because the large-scale fields are still growing due to resistive dissipation of small-scale helicity.

3.4 Growth of the large-scale field

We define the strength of the large-scale field $\overline{B}(t)$, by integrating the energy spectrum $E_M(k, t)$ between $k = 1-2$ and equating this to $\overline{B}^2/2$. The ratio of strength of this large-scale field relative to the rms field $\overline{B}(t)/B_{\text{rms}}$ is shown in Figure 9 evolving from the kinematic stage to nonlinear sat-

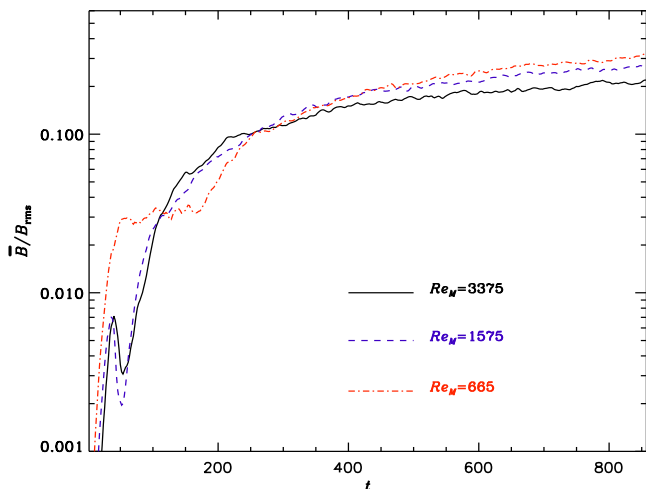


Figure 10. The ratio \bar{B}/B_{rms} is evolving with time, for Runs D, E, and F.

uration, for Runs A, B, and C. For the fiducial Run A, shown as a solid black line, $\bar{B}/B_{\text{rms}} \sim 0.04\text{--}0.05$ in the kinematic stage. This is a factor 2 larger than \bar{B}/B_{rms} determined by SB14 (Fig. 6) on the basis of the mean power in horizontally averaged fields. However we find that in the kinematic stage, the ratio \bar{B}/B_{rms} in fact decreases with Re_M approximately as $\text{Re}_M^{-3/4}$, which agrees with the scaling found by SB14 for the horizontally averaged mean field.

The ratio \bar{B}/B_{rms} begins to increase rapidly once the small-scale field starts saturating, at $t \sim 400$ for Run A. This reflects the fact that, while the large k modes saturate, the $k = 1, 2$ modes which determine \bar{B} , continue to grow due to large-scale dynamo action. This can also be seen explicitly in the inset of Figure 9, where B_{rms} in solid black turns to saturate at around $t = 400$ while \bar{B} in dashed blue continues to grow, again reflecting the continued efficiency of the mean (large-scale) field dynamo even when the fluctuation dynamo begins to saturate. Finally, after $t = 600$, this ratio enters a phase of slower growth; at this stage basically the large-scale field becomes more and more dominant as the helicity of the small-scale field is lost due to resistive dissipation. Note that, although larger k modes begin to saturate by $t = 400$ as was seen earlier also in Figure 2, modes closer to the forcing scale (for example the mode in M_4 , also shown again in dashed red in the bottom panel of Figure 9) are growing at the same rate as the modes in $k = 1, 2$ between $t = 400$ to 500 and they turn to saturate at nearly the same time, thus reinforcing the picture of a unified dynamo. But from $t = 600$ onwards, while the modes equal to $k = 4$ and larger saturate completely, the $k = 1, 2$ modes continue to grow on resistive time scales. By the end of our run we have $\bar{B}/B_{\text{rms}} \sim 0.4$, for the fiducial run. The lower Re_M runs develop an even higher value of $\bar{B}/B_{\text{rms}} \sim 0.5$ and 0.6 , for $\text{Re}_M = 160$ and 65 , respectively. This larger \bar{B}/B_{rms} for lower Re_M arises because the resistive dissipation of helicity is more important in these cases.

We show the evolution of the ratio \bar{B}/B_{rms} also in the case of $\text{Pr}_M = 10$ in Figure 10 for Runs D, E, and F. Here again the ratio \bar{B}/B_{rms} increases dramatically from the kinematic to the saturation regime. We can assess how the scaling of the ratio \bar{B}/B_{rms} vs. Re_M^ζ changes from the kinematic

to the saturation regime. In the former case of $\text{Pr}_M = 0.1$, ζ changes from a value of ~ -0.75 in the kinematic phase to ~ -0.2 during saturation. In the case of $\text{Pr}_M = 10$, the kinematic phase is rather short in the current runs, but one can see that ζ again tends to a small value of about -0.2 upon saturation. The small residual Re_M dependence of \bar{B}/B_{rms} is also expected to disappear in the final saturated state of the α^2 dynamo, where one expects this ratio to tend towards $(k_f/k_1)^{1/2}$, provided the small scale helicity can be lost effectively (Brandenburg 2001). In the current simulations as the helicity is only lost resistively, this has not yet occurred. All in all, we see that a significant large scale field can be generated even in the presence of an active fluctuation dynamo. By the time they saturate the curves come closer together indicating that the mean field is dominant now.

4 DISCUSSION

Using high resolution DNS, we have shown that, for helical turbulence at large Re_M , the mean-field dynamo works efficiently to generate significant large-scale fields – even in the presence of a strong fluctuation dynamo. It appears that there is only one unified large/small-scale dynamo in such helical turbulence where initially fields on all scales grow together, and when the Lorentz force becomes important, successively larger scales saturate.

4.1 Shape-invariant growth of the spectrum

As in SB14, we find that in the kinematic stage the spectrum grows as a shape-invariant eigenfunction of the helical dynamo, peaked at small scales (or large k). There is clear evidence for a large-scale field even at this stage, seen as excess power at small k in the negatively polarized component of the energy spectrum. However, the ratio of the strength of this large-scale field to the rms field decreases with increasing Re_M . This is due to efficient fluctuation dynamo action, which amplifies power at small (nearly resistive) scales. The question then arises whether, in the presence of a fluctuation dynamo, the large-scale field can grow to a significant fraction of the rms field – at least when the dynamo saturates.

4.2 Scale-dependent saturation of the unified dynamo

We show from the evolution of the spectra (Figures 1 and 2) that, as the field grows, small scales (large k modes, $k > 4$) saturate first, but the large-scale field (with $k = 1$) continues to grow at about the same rate as the $k = 4$ mode, even when this happens. This can be seen by examining the wavelength-dependent growth rate of both the differently polarized components (Figure 4) and the total field (Figure 5). These $\lambda(k)$ start out as being independent of k in the kinematic stage, but progressively decrease to zero, first at large k and then at smaller and smaller k . This saturation behavior where small scales saturate first and then larger and larger scales saturate, remains qualitatively unchanged for $\text{Pr}_M = 10$, even though the small scale dynamo is more efficient, as can be seen in Figure 3.

4.3 Increase of small-scale field coherence

At the end of our simulation, the spectra displays two peaks, one at the forcing wavenumber k_f , and the other at $k = 1$. Therefore the back reaction due to the Lorentz force has enabled the small-scale field coherence to increase from small scales to the forcing scale, and at the same time allowed the large-scale field to develop.

The first feature can also be seen from Figures 6 and 7, where we show the evolution of the integral scale L_{int}^+ of the positively polarized component (identified with the small-scale field). For our fiducial Run A ($\text{Pr}_M = 0.1$), we show that L_{int}^+ evolves from a value of ~ 0.17 in the kinematic stage to $L_{\text{int}}^+ \sim 0.9$ upon saturation, a significant fraction of the forcing scale ($2\pi/k_f$). Also in the case of $\text{Pr}_M = 10$, as in Run D, L_{int}^+ increases by a factor of ~ 8 . In fact, through nonlinear saturation, the small-scale field has become as coherent as possible for the given forcing scale.

4.4 Significant growth of large scale field upon saturation

The growth of the large-scale field to significant levels, even in the presence of the fluctuation dynamo, was also shown by considering the time evolution of $\overline{B}/B_{\text{rms}}$ (see Figures 9 and 10). This ratio, in the case of $\text{Pr}_M = 0.1$, starts from a small value of ~ 0.04 during the kinematic stage, but at the end of our run, we obtain a significant large-scale field with $\overline{B}/B_{\text{rms}} \sim 0.4$. A large increase in this ratio is seen for also Runs D, E, and F with $\text{Pr}_M = 10$. The growth of the ratio in Run A occurs in two stages: First between $t \sim 400$ – 600 there is a rapid growth of $\overline{B}/B_{\text{rms}}$ as the fluctuation dynamo saturates. It appears that the nonlinear ordering effects of the Lorentz force that saturate the small-scale fields, still allow growth of progressively larger scale fields, including scales larger than the forcing scale at $k < 4$. For $t > 600$, there is a slower growth of $\overline{B}/B_{\text{rms}}$ presumably driven by the resistive dissipation of the small-scale helicity. It would be interesting to ask if, in very large Re_M astrophysical systems, the effect of this resistive dissipation of small-scale helicity can also be achieved by having instead magnetic helicity fluxes (Blackman & Field 2000; Kleeorin et al. 2000).

4.5 Quantum mechanical analogy

It may be instructive to think in terms of the Kazantsev model incorporating helicity (Subramanian 1999; Boldyrev et al. 2005; Subramanian & Brandenburg 2014), where the dynamo problem is mapped to a quantum mechanical potential problem, with growing small-scale dynamo modes mapped to bound states in the potential and with helicity allowing for tunnelling to have enslaved large-scale field correlations with the same growth rate. The effect of the Lorentz force could be to make the potential well at the small scale k_f^{-1} to become shallower, allowing for only the marginally bound state to exist, while still having sufficient depth at the large scale k_1^{-1} , to allow the tunnelling free-particle states to grow.

Such behavior is indeed obtained in a related real-space double-well potential problem, arising in non-axisymmetric galactic dynamos, where the dynamo is enhanced along a spiral (Chamandy et al. 2013a,b). There the potential wells

are near the galactic center and the corotation radius of the spiral. The fastest growing kinematic eigenfunction is largest in the central regions. But its tail is enhanced along the magnetic spiral, near corotation radius. However, saturation of the field near the galactic center, still allows for the field to grow around corotation and become significant. From our work here, it appears that such a situation can also be obtained for a double-well potential in ‘scale’ or wavenumber space, when one incorporates nonlinear saturation effects. It would be of interest to demonstrate this also in a nonlinear version of the Kazantsev model, perhaps generalizing the work of Subramanian (1999); Brandenburg & Subramanian (2000) to include helicity loss.

4.6 The very limited role of α effect growth rates

In the early days of mean-field dynamo theory, computing linear growth rates was about the only way different dynamo modes could be characterized. In the late 1980s, their limited usefulness became clear. Only the marginally excited case of zero growth rates remained truly useful. In particular, the dominance of one mode over the other is entirely determined by nonlinearity, and not at all by differences in their kinematic growth rates (Brandenburg et al. 1989).

Linear growth rates have traditionally also been used to estimate the time it takes for the large-scale dynamo to reach saturation. The linear growth rate of the α^2 large-scale dynamo is expected to be much smaller than that of the small-scale dynamo. We have seen however that all modes grow together in the kinematic stage, and large-scale modes at $k = 1$ – 2 continue to grow at the same rapid rate even when the small-scale modes ($k > 4$) saturate. Note that it is the linear growth rate which has been important in discussions of the strength of the large-scale field in young galaxies (Kronberg et al. 1992; Bernet et al. 2008; Joshi & Chand 2013; Farnes et al. 2014). Our present work does not really apply to galaxies, where shear is also important and the magnetic Prandtl number is large, but it highlights quite clearly that any estimate based on the value of α , or the value of $|\alpha \nabla \Omega|^{1/2}$ in models with differential rotation Ω (Beck et al. 1996) must be irrelevant. This was in principle already recognized by Beck et al. (1994), who invoked a small-scale dynamo at early times to kick-start the large-scale dynamo at later times.

In galaxies, the turnover time on the integral scale can be as short as 10^6 or 10^7 years, but with fluid Reynolds numbers well above 10^7 , the relevant e -folding time of dynamo growth will be shortened by a factor of $\text{Re}^{1/2} \approx 3 \times 10^3$ or more. Based on this argument, galactic dynamos may reach saturation first at the smallest eddy scales, on a time scale as short as several hundred years. A relevant limitation of reaching coherent large-scale fields comes only from the late saturation phase when magnetic helicity fluxes are expected to play an important role.

5 CONCLUSIONS

The results presented here support the idea that large-scale fields can be efficiently generated even in the presence of strongly growing fluctuations driven by the fluctuation dynamo. Clearly, the growth of the larger scale field is aided

by the presence of helicity in the turbulence. But it is not as if there is an α^2 large-scale dynamo independent of the small-scale dynamo; as the growth rate of the $k = 1$ mode does not seem to change significantly right from the kinematic to the nonlinear stage. Rather it appears that there is one unified dynamo, with all scales initially growing together at one rate, and then the largest scales continuing to grow (aided by small-scale magnetic helicity loss) as the small-scale fields saturate.

Several extensions of our model can be envisaged. Our dynamo is a homogeneous one, making catastrophic (resistive) quenching effects more pronounced. It would therefore be useful to extend our studies to inhomogeneous systems, for example when there is shear. In that case, the magnetic energy density of the mean magnetic field, \overline{B}^2 , is no longer constant in space, which leads to a nonuniformity of the magnetic helicity flux divergence and can thereby alleviate catastrophic (premature) quenching, as was shown by Hubbard & Brandenburg (2012). Such models should therefore be studied more thoroughly. However, as astrophysical systems are all confined in space with a corona and low-density material outside, it would be useful to address such systems in some fashion. It would be interesting to see whether this could remove the slow-down of the growth caused by total magnetic helicity conservation during the saturation phase. This would be particularly important in view of understanding the observed levels of coherent magnetic fields in young galaxies.

ACKNOWLEDGMENTS

We acknowledge the usage of the high performance computing facility at IUCAA. PB acknowledges SRF support from CSIR, India and currently from DOE, DE-FG02-12ER55142, at Princeton, USA. This work was supported in part by the Swedish Research Council grants No. 621-2011-5076 and 2012-5797, as well as the Research Council of Norway under the FRINATEK grant 231444.

REFERENCES

Beck R., Brandenburg A., Moss D., Shukurov A., Sokoloff D., 1996, *Ann. Rev. Astron. Astrophys.*, 34, 155
 Beck R., Poezd A. D., Shukurov A., Sokoloff D. D., 1994, *A&A*, 289, 94
 Bernet M. L., Miniati F., Lilly S. J., Kronberg P. P., Dessauges-Zavadsky M., 2008, *Natur*, 454, 302
 Bhat P., Subramanian K., 2013, *MNRAS*, 429, 2469
 Blackman E. G., 2015, *SSRv*, 188, 59
 Blackman E. G., Field G. B., 2000, *MNRAS*, 318, 724
 Boldyrev S., Cattaneo F., Rosner R., 2005, *Phys. Rev. Lett.*, 95, 255001
 Brandenburg A., 2001, *ApJ*, 550, 824
 Brandenburg A., 2003, in Ferriz-Mas A., Núñez M., eds, *Advances in Nonlinear Dynamos Computational aspects of astrophysical MHD and turbulence*. Taylor & Francis, London and New York, pp 269–344
 Brandenburg A., 2011, *ApJ*, 741, 92
 Brandenburg A., Dobler W., 2002, *Computer Physics Communications*, 147, 471

Brandenburg A., Dobler W., Subramanian K., 2002, *Astron. Nachr.*, 323, 99
 Brandenburg A., Krause F., Meinel R., Moss D., Tuominen I., 1989, *A&A*, 213, 411
 Brandenburg A., Sokoloff D., Subramanian K., 2012, *SSRv*, 169, 123
 Brandenburg A., Subramanian K., 2000, *A&A*, 361, L33
 Brandenburg A., Subramanian K., 2005, *PhR*, 417, 1
 Chamandy L., Subramanian K., Shukurov A., 2013a, *MNRAS*, 428, 3569
 Chamandy L., Subramanian K., Shukurov A., 2013b, *MNRAS*, 433, 3274
 Falkovich G., 1994, *Physics of Fluids*, 6, 1411
 Farnes J. S., O’Sullivan S. P., Corrigan M. E., Gaensler B. M., 2014, *ApJ*, 795, 63
 Haugen N. E., Brandenburg A., Dobler W., 2004, *PRE*, 70, 016308
 Hubbard A., Brandenburg A., 2012, *ApJ*, 748, 51
 Isakov A. B., Schekochihin A. A., Cowley S. C., McWilliams J. C., Proctor M. R. E., 2007, *Phys. Rev. Lett.*, 98, 208501
 Joshi R., Chand H., 2013, *MNRAS*, 434, 3566
 Kazantsev A. P., 1968, *Sov. J. Exp. Theor. Phys.*, 26, 1031
 Kleeorin N., Moss D., Rogachevskii I., Sokoloff D., 2000, *A&A*, 361, L5
 Kronberg P. P., Perry J. J., Zukowski E. L. H., 1992, *ApJ*, 387, 528
 Kulsrud R. M., Anderson S. W., 1992, *ApJ*, 396, 606
 Schekochihin A. A., Cowley S. C., Taylor S. F., Maron J. L., McWilliams J. C., 2004, *ApJ*, 612, 276
 Subramanian K., 1999, *Phys. Rev. Lett.*, 83, 2957
 Subramanian K., Brandenburg A., 2014, *MNRAS*, 445, 2930
 Tobias S. M., Cattaneo F., Boldyrev S., 2011, *arXiv*: 1103.3138
 Vainshtein S. I., Kichatinov L. L., 1986, *JFM*, 168, 73